JCTC Journal of Chemical Theory and Computation

Article

pubs.acs.org/JCTC

A Comparison of Advanced Monte Carlo Methods for Open Systems: CFCMC vs CBMC

Ariana Torres-Knoop,[†] Sayee Prasaad Balaji,[‡] Thijs J. H. Vlugt,[‡] and David Dubbeldam*[,†]

[†]Van't Hoff Institute for Molecular Sciences, University of Amsterdam, Science Park 904, 1098 XH Amsterdam, The Netherlands

[‡]Process & Energy Department, Delft University of Technology, Leeghwaterstraat 39, 2628CB Delft, The Netherlands

Supporting Information

ABSTRACT: Two state-of-the-art simulation methods for computing adsorption properties in porous materials like zeolites and metal−organic frameworks are compared: the configurational bias Monte Carlo (CBMC) method and the recently proposed continuous fractional component Monte Carlo (CFCMC) method. We show that CFCMC is a very significant improvement over CBMC, and we can recommend it as our preferred method of choice. It is faster, more reliable, and (in contrast to CBMC) provides insight on whether or not the results are properly equilibrated. We also show that it is possible to combine the methods in a new CB/CFCMC hybrid method and derive the acceptance rules. This method achieves even higher insertion acceptance ratios.

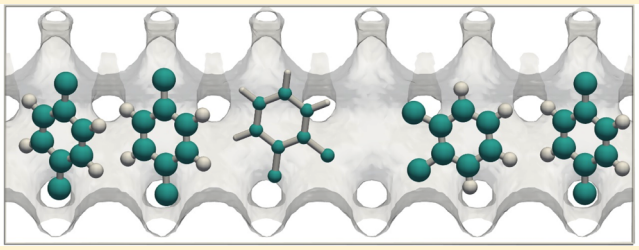

1. INTRODUCTION

When studying adsorption properties of materials, we are interested in the amount of molecules adsorbed (e.g., in units of mol/kg) as a function of the pressure and temperature. Computational studies, usually using Monte Carlo (MC) simulations, mimic this situation by attempting to insert and delete particles into and from the system in the grand canonical ensemble or μ, V, T ensemble.[1−3] In this ensemble, the chemical potential μ, volume V, and temperature T are fixed. The fixed volume V follows from the definition and volume of the studied crystal structure, and the chemical potential μ can be directly related to the fugacity, which is obtained using an equation of state from the pressure. Because the chemical potential is fixed, the number of molecules fluctuates. Therefore, the property that is computed is the average number of molecules per unit of volume. A system where the number of molecules varies is called an *open system*. All open ensembles methods suffer from a major drawback; the probability that an insertion/deletion is accepted becomes vanishingly low at higher densities due to overlaps with the host structure and/or molecules that are already adsorbed. This makes it difficult to accurately compute the maximum loading of molecules in a structure (which is required in theoretical models like the Langmuir model).

To increase the number of successfully inserted molecules, the configurational bias Monte Carlo (CBMC) technique was developed.[2,4,5] In CBMC, instead of generating ideal gas configurations and trying to insert the molecule as a whole, chains are inserted segment by segment where the growth process is biased toward energetically favorable configurations. The scheme is therefore able to avoid (or at least reduce the amount of) configurations that overlap with the framework and other particles. This scheme also works for configurations of long molecules that become increasingly different from the gas phase as a function of chain length.

The CBMC method starts to have problems at medium densities and fails at high densities.[3] A new scheme to remedy this problem is the continuous fractional component Monte Carlo (CFCMC) method of Shi and Maginn.[6−8] In this method, the system is expanded with a single "fractional" molecule per component type that has a scaled interaction with the other molecules and with the framework. The scaling parameter λ ranges from 0 to 1, with $\lambda = 0$ meaning the molecule is not felt by the surroundings (i.e., the host structure and remaining molecules), while $\lambda = 1$ means the molecule is fully present and the interactions with the surrounding are at full strength. In addition to the usual set of MC moves, moves are now also performed on λ, attempting to increase and decrease it. Effectively, increasing λ corresponds to "inflating" the molecule, and decreasing λ corresponds to "deflating" the molecule. A change of λ larger than 1 leads to insertion of a new chain. The fractional molecule is made an integer, and a new molecule is randomly inserted into the system with the remainder of λ. This is the new fractional molecule. Similarly, a decrease in λ below zero leads to deletion of a molecule. Further details are provided in the Methodology section. The crucial point to note here, however, is that the λ moves can be biased, ideally making the λ histogram flat. The method therefore is able to *force* molecules in and out of the system, thereby allowing the open ensemble to be efficiently implemented in a simulation.

There are few papers investigating the use of CFCMC for adsorption simulations. In ref 3, we previously showed excellent

Received: November 8, 2013
Published: February 3, 2014

agreement between CFCMC and CBMC for a few simple cases, for example, single component adsorption isotherms of small guest molecules in several zeolites and MOFs. In this work, we compare CFCMC and CBMC in more complex scenarios: alkanes in $Fe_2(BDP)_3$, adsorption of small rigid guest molecules in MgMOF-74, and xylenes in MTW-type zeolite. In addition, we show that the methods are easily combined in a CB/CFCMC hybrid method. We evaluate this method with simulations in the grand canonical and Gibbs ensemble, and in the Supporting Information, this method is derived in detail. The algorithms are implemented in our in-house RASPA code.[9] We will show that CFCMC is a very significant improvement over conventional MC and even over CBMC.

2. METHODOLOGY

2.1. Configurational Bias Monte Carlo (CBMC). The CBMC framework is based on work by Rosenbluth and Rosenbluth[5] and developed by a variety of researchers.[4,10−15] In the CBMC scheme, it is convenient to split the total potential energy U of a segment of a molecule into two parts

$$U = U^{\text{int}} + U^{\text{ext}} \tag{1}$$

The first part of the potential, the internal bonded potential U^{int}, is used for the generation of trial positions. The second part, the external potential U^{ext}, is used to bias the selection of a site from the a set of trial positions. This bias is exactly removed by adjusting the acceptance rules. In the CBMC technique, a molecule is grown segment-by-segment. For each segment, a set of k trial positions is generated according to the internal energy U^{int}. The number of trial positions k is usually between 10 and 20. For each trial position j of segment i, the external energy $U_i^{\text{ext}}(j)$ is computed. One of these trial positions is selected with a probability proportional to its Boltzmann factor

$$P_i(j) = \frac{\exp[-\beta U_i^{\text{ext}}(j)]}{\sum_{l=1}^{k}\exp[-\beta U_i^{\text{ext}}(l)]} = \frac{\exp[-\beta U_i^{\text{ext}}(j)]}{w(i)} \tag{2}$$

where $\beta = 1/k_{\text{B}}T$ is the inverse temperature, and k_{B} is the Boltzmann factor. The selected trial position is added to the chain, and the procedure is repeated until the entire molecule has been grown. For this newly grown molecule, the Rosenbluth factor of the new configuration W^{new} is computed

$$W^{\text{new}} = \prod_{i=1}^{n} w(i) \tag{3}$$

in which n is the number of segments in the chain. To compute the old Rosenbluth factor W^{old} of an already existing chain, $k-1$ trial positions are generated for each segment. These positions, together with the already existing position, form the set of k trial positions.

The acceptance rules for CBMC insertion and deletion moves in the grand canonical ensemble are given by[2]

$$\text{acc}(N \rightarrow N+1) = \min\left(1, \frac{f\beta V}{N+1}\frac{W^{\text{new}}}{\langle W^{\text{IG}}\rangle}\right) \tag{4}$$

$$\text{acc}(N \rightarrow N-1) = \min\left(1, \frac{N}{f\beta V}\frac{\langle W^{\text{IG}}\rangle}{W^{\text{old}}}\right) \tag{5}$$

in which $\langle W^{\text{IG}}\rangle$ is the average Rosenbluth factor of an isolated molecule in the gas phase, f is the fugacity, V is the volume, and N is the number of molecules. The pressures and fugacities are related via the equation of state of the gas phase. The "reinsertion" move removes a randomly selected molecule and reinserts it at a random position. For rigid molecules, it uses orientational biasing,[3] and for chains, the molecule is fully regrown (the internal configuration is modified). To properly sample the internal structure (i.e., bond/bend/torsions), the "partial reinsertion" move is useful. Several atoms of the molecule are kept fixed, while others are regrown. Because there is already space for the atoms, the acceptance ratios are high. The acceptance rule for full and partial regrowth is given by

$$\text{acc}(\text{old} \rightarrow \text{new}) = \min\left(1, \frac{W^{\text{new}}}{W^{\text{old}}}\right) \tag{6}$$

For mixtures, especially at higher density, the "identity switch" move becomes crucial. The identity change trial move[16−19] is called the semi-grand ensemble. One of the components is selected at random, and an attempt is made to change its identity. The acceptance rule is given by[16]

$$\text{acc}(A \rightarrow B) = \min\left(1, \frac{W^{\text{new}} f_B \langle W_A^{\text{IG}}\rangle N_A}{W^{\text{old}} f_A \langle W_B^{\text{IG}}\rangle (N_B+1)}\right) \tag{7}$$

where f_A and f_B are the fugacities of components A and B, and N_A and N_B are the number of particles.

Since the introduction of CBMC, the method has been extended to include growpaths for branched molecules,[2,20−26] cyclic molecules,[27−30] and reactive CBMC.[31,32]

2.2. Continuous Fractional Component Monte Carlo (CFCMC). CFCMC was developed by Shi and Maginn[6] inspired by a group of schemes known as "expanded ensembles".[33,34] The system is expanded with an additional particle, where interactions with the surrounding molecules are scaled using a parameter λ. Various choices for the scaling are possible. In the original CFCMC method, and also in this work, Lennard−Jones (LJ) interactions $u_{\text{LJ}}(r)$ and charge−charge interactions u_{Coul} are scaled as

$$u_{\text{LJ}}(r) = \lambda 4\varepsilon\left[\frac{1}{\left[\frac{1}{2}(1-\lambda)^2 + \left(\frac{r}{\sigma}\right)^6\right]^2} - \frac{1}{\left[\frac{1}{2}(1-\lambda)^2 + \left(\frac{r}{\sigma}\right)^6\right]}\right] \tag{8}$$

$$u_{\text{Coul}} = \lambda^5 \frac{1}{4\pi\varepsilon_0}\frac{q_i q_j}{r} \tag{9}$$

where ε_0 is the dielectric constant in vacuum, r is the interatomic distance, q is the atomic charge, ε is the LJ strength parameter, and σ is the LJ size parameter.

The modified form of the conventional LJ potential forces the potential to remain finite when $r \rightarrow 0$ for $\lambda \neq 1$. The scaled potential has the correct behavior at the limits of $\lambda = 0$ and $\lambda = 1$, i.e., for $\lambda = 0$ there are no interactions, and for $\lambda = 1$ the conventional LJ and Coulombic interactions are recovered. Note that only the intermolecular energy (U^{inter}) is scaled. Many variations on the algorithm are possible. For example, λ can be changed per molecule or per atom. In any case, the method slowly "inflates" and "deflates" the molecule like a balloon.

CFCMC uses conventional MC for thermalization (such as translations, rotations, and/or MC-MD hybrid moves[35,36]) but, in addition, attempts to change λ of the fractional molecule

dx.doi.org/10.1021/ct4009766 | J. Chem. Theory Comput. 2014, 10, 942−952

using $\lambda(n) = \lambda(o)+\Delta\lambda$. The value of $\Delta\lambda$ is chosen uniformly between $-\Delta\lambda^{max}$ and $+\Delta\lambda^{max}$ and adjusted to achieve approximately 50% acceptance. However, many systems show behavior where λ changes are difficult[3,6,7] because in the Boltzmann ensemble the distribution of λ can go through a deep minimum. An additional bias η on λ can be used, where each state of λ has an associated biasing factor η. This bias will be removed by the acceptance rules. A careful calibration of η will make the λ histograms flat and hence can avoid situations where the system gets stuck in a certain λ range. There are three possible outcomes of a change from $\lambda(o)$ to $\lambda(n)$:

(1) $\lambda(n)$ remains between 0 and 1:

The change in energy of the particle with the new $\lambda(n)$ compared to the old energy is computed and the move is accepted using

$$P_{acc} = \min(1, \exp[-\beta(U_{inter}(n) - U_{inter}(o)) + \eta(\lambda(n)) - \eta(\lambda(o))]) \quad (10)$$

There is no change in the number of particles, positions, or in the intramolecular energies. Only λ and the intermolecular energy are changed.

(2) $\lambda(n)$ becomes larger than 1:

When $\lambda(n)$ exceeds unity, i.e., $\lambda(n) = 1 + \varepsilon$, the current fractional molecule is made fully present ($\lambda = 1$), and an additional particle is randomly inserted with $\lambda = \varepsilon$. In the original paper,[6] an ideal gas molecule is taken form a reservoir of equilibrated gas-phase molecules stored in the memory of the computer. In our implementation, the ideal gas molecule is generated "on the fly" during the simulation.

(3) $\lambda(n)$ becomes smaller than 0:

When $\lambda(n)$ falls below 0, i.e., $\lambda(n) = -\varepsilon$, the current fractional molecule is removed from the system ($\lambda = 0$), and a new fractional molecule is chosen with $\lambda = 1 - \varepsilon$.

The acceptance rules for insertion and deletion in the grand canonical ensemble the rules are given by[3,6]

$$P_{acc}(N \to N+1) = \min\left(1, \frac{f\beta V}{N+1}\exp[\eta(\lambda(n)) - \eta(\lambda(o))] \exp[-\beta(U_{inter}(n) - U_{inter}(o))]\right) \quad (11)$$

$$P_{acc}(N \to N-1) = \min\left(1, \frac{N}{f\beta V}\exp[\eta(\lambda(n)) - \eta(\lambda(o))] \exp[-\beta(U_{inter}(n) - U_{inter}(o))]\right) \quad (12)$$

where N is the number of *integer* molecules. Hence, measured properties and loadings should exclude the fractional molecule.

The CFCMC method is able to force molecules into and out of the system. If the molecule is too quickly removed after insertion, then nothing is gained. The environment should be able to adjust to the new insertion and equilibrate properly. The adjustment is also called thermalization. CFCMC uses conventional MC moves such as translation, rotation, and/or MC-MD hybrid moves for thermalization. In our implementation, we also use (partial-)reinsertion moves using configurational biasing (identical to CBMC) for both integer molecules and the fractional molecules. The insertion of an additional molecule is already biased using λ biasing, and as soon as the molecule is present in the system, the reinsertion is able to efficiently move the molecules around in the system. For mixtures, we use the identity switch move but only on integer molecules because each component should always have one and only one fractional molecule.

Shi and Maginn found that Wang–Landau sampling is very efficient in obtaining the biasing factors for CFCMC,[6−8] and our experience confirms this. The objective of the Wang–Landau sampling method[37,38] is to make all system energy states equally probable. In CFCMC, this translates in making all system λ states equally probable. During a random walk, the weights are iteratively adjusted using importance sampling. The λ range is, for example, divided into 20 bins. Initially all biasing factors are zero. During equilibration, the bin corresponding to the current λ is modified according to $\eta(\lambda_j) \to \eta(\lambda_j) - \nu$ after a MC move attempt, where ν is a scaling parameter initially set to 0.01. Histograms are measured, and every 10000 attempts checked for flatness. The histogram is considered sufficiently flat when all bins are at least 30% as often visited as the most visited bin. If so, then the histograms are set to zero, and the scaling factor is modified to $\nu \to (1/2)\nu$. Equilibration of η can be stopped once the value of ν is lower than 10^{-6}.

2.3. CB/CFCMC. The insertion and deletion scheme of CFCMC can in certain cases be improved by fractionally growing and retracing a molecule at a fixed λ using CBMC. In the Supporting Information, we derive the acceptance rules for the continuous fractional component Monte Carlo method combined with configurational bias Monte Carlo (CB/CFCMC). In this method, new chains are inserted and old chains are removed using configurational biasing at constant λ values. When $\lambda = 1$ or $\lambda = 0$, the algorithm reduces to conventional CBMC for insertion and deletion, respectively. The algorithm is applied to the Gibbs ensemble. Application to the grand canonical ensemble is straightforward and can be effected by taking one of the simulation boxes as an infinitely large reservoir of noninteracting chain molecules. In the Supporting Information, we prove that the $\exp[-\beta\Delta U]$ term in eqs 11,12 should be replaced with $W(n)/\langle W^{IG}\rangle$ for insertion and by $\langle W^{IG}\rangle/W(o)$ for deletion.

The procedure for insertion/deletion attempts in the grand canonical ensemble is:

- **insertion**, $\lambda_n = 1 + \varepsilon$

(1) Unbiased: the fractional molecule with $\lambda = \lambda_o$ is made integer ($\lambda = 1$), and the energy difference ΔU is computed.

(2) Biased: a new fractional molecule with $\lambda_n = \varepsilon$ is grown using CBMC giving $W(n)$.

(3) Acceptance rule: $P_{acc} = \min(1, f\beta V/(N+1)\ W(n)/\langle W^{IG}\rangle \exp[-\beta\Delta U]\exp[\eta(\lambda(n)) - \eta(\lambda(o))])$

- **deletion**, $\lambda_n = -\varepsilon$

(1) Biased: the existing fractional particle is retraced using CBMC with $\lambda = \lambda_o$ giving $W(o)$, and the fractional molecule is subsequently removed.

(2) Unbiased: A new fractional molecule is randomly chosen with $\lambda_n = 1 - \varepsilon$, and the energy difference ΔU is computed.

(3) Acceptance rule: $P_{acc} = \min(1, N/f\beta V\ \langle W^{IG}\rangle/W(o) \exp[-\beta\Delta U]\exp[\eta(\lambda(n)) - \eta(\lambda(o))]$

We tested the CB/CFCMC method by computing the single component and mixture adsorption isotherms of hexane isomers in $Fe_2(BDP)_3$ at 433K (Figure S1, Supporting Information). The isotherms computed using CB/CFCMC, CBMC and CFCMC are equivalent within statistical error.

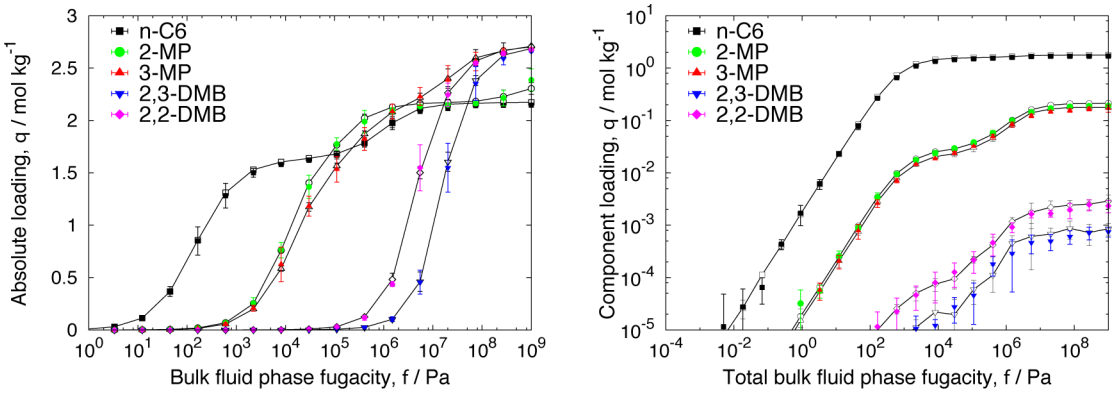

Figure 1. Adsorption isotherms calculated using CFCMC (closed symbols) and CBMC (open symbols). (a) Single-component isotherms of hexane isomers in Fe2BDP3 at 433 K. (b) Five-component mixture of hexane isomers in Fe2BDP3 at 433 K. (hexane = n-C6, 2-methylpentane = 2-MP, 3-methylpentane = 3-MP, 2,2-dimethylbutane = 2,2DMB, and 2,3-dimethylbutane = 2,3DMB). The results are also in good agreement with CB/CFCMC (Figure S1, Supporting Information).

2.4. Using Energy/Force Tabulation. Host frameworks can show large structural changes induced by pressure, temperature, and/or loading effects. In the absence of these structural changes, there is surprisingly little influence of framework flexibility on adsorption.[39] Computationally, it is convenient to keep the framework fixed because the potential energy surface of the framework can be precomputed,[40,41] for example, using a three-dimensional cubic Hermite polynomial interpolation algorithm.[42] Instead of looping over all framework atoms in order to compute the host adsorbate energy, one can perform a single 3D grid interpolation. The more points that are in the grid, the higher the accuracy is.

In this work, we use the triclinic grid interpolation scheme in three dimensions of Lekien and Marsden.[43] The algorithm is based on a specific 64 × 64 matrix (the C code is available online in the link in ref 43, but for convenience, the matrix and pseudocode are also listed in the Supporting Information) that provides the relationship between the derivatives at the corners of the elements and the coefficients of the tricubic interpolant for this element. The cubic interpolant and its first three derivatives are continuous and consistent. The same grids can therefore be used for both MC and MD with no additional energy drift besides the drift due to the integration scheme,that is, the energy gradients are the *exact* derivatives of the energy at each point in the element. The required storage is a set of the local potential energy U and its first, second, and third derivatives

$$\left\{U, \frac{\partial U}{\partial x}, \frac{\partial U}{\partial y}, \frac{\partial U}{\partial z}, \frac{\partial^2 U}{\partial x \partial y}, \frac{\partial^2 U}{\partial x \partial z}, \frac{\partial^2 U}{\partial y \partial z}, \frac{\partial^3 U}{\partial x \partial y \partial z}\right\} \quad (13)$$

for each grid point. The energy and forces at a point in an element are computed from the surrounding eight corner points. That is, tricubic local interpolation uses only data in the neighborhood of an element. The problem is not separated into three one-dimensional problems as is conventionally done.[44] We implemented the algorithm in Cartesian space. For triclinic unit cells, a rectangular cell enclosing the unit cell is used. In general, a grid spacing of 0.1 Å can be considered as high accuracy, 0.15 Å as medium accuracy and 0.2 Å as a coarse grid. However, this is system dependent (e.g., on the framework density). To assess the accuracy of the grid, a large number of test insertions are done at random positions. The energy difference between the grid interpolation and the actual (fully computed) energy evaluation is Boltzmann weighted because an energy difference at high energies is much less important than in the low energy regions. We consider a grid "good enough" when the Boltzmann weighted average relative energy difference is smaller than 10^{-3}. Then, there are no detectable differences in computed properties using energy/force grids or full energy/force evaluations.

Note that for each type of atom, a separate van der Waals grid needs to be precomputed and stored. However, grids can sometimes be combined. For example, for the Lennard–Jones potential, atom types that have the same size parameter σ can use the same grid and the term with the strength parameter ε serves as a post-multiplication factor.[23] The same applies to the Coulombic grid. The grid is created using a test charge of $+1e$, and only one charge-grid is needed. We use the Ewald summation for charge–charge interactions, and the grid stores only the real part of the Ewald potential. The Fourier part (using wave vectors $\mathbf{k}$) is handled on the fly, but also in this case, $\mathbf{k}$ sums over atoms that do not move, that is, the rigid host framework, are precomputed at the start of the simulation.[45] Lastly, we would like to note that grids can also be used for CFCMC. For Coulombic interactions, one can use a grid for the fractional molecule, as one simply multiplies the grid by a factor λ[5] (eq 9). However for the LJ interactions, due to the λ-dependent terms in the modified potential (eq 8), the energy of the fractional molecule has to be computed either in a conventional way or using grids for different values of λ. The latter option is impeded by large memory requirements (and therefore, the slowdown of the code). Still, the speed up of using grids in CFCMC is almost the same as CBMC because there are only a few fractional adsorbates (i.e., one fractional molecule per component) and many integer adsorbates. In our experience, the speedup factor of using grids compared to full host adsorbate energy/force evaluations lies roughly in the order of 5–25, depending on the amount of framework atoms, type of adsorbates, and loading (adsorbate–adsorbate interactions are still computed fully).

3. RESULTS

3.1. Alkanes in $Fe_2(BDP)_3$. The separation of linear, monobranched, and dibranched isomers of alkanes is of

dx.doi.org/10.1021/ct4009766 | J. Chem. Theory Comput. 2014, 10, 942–952

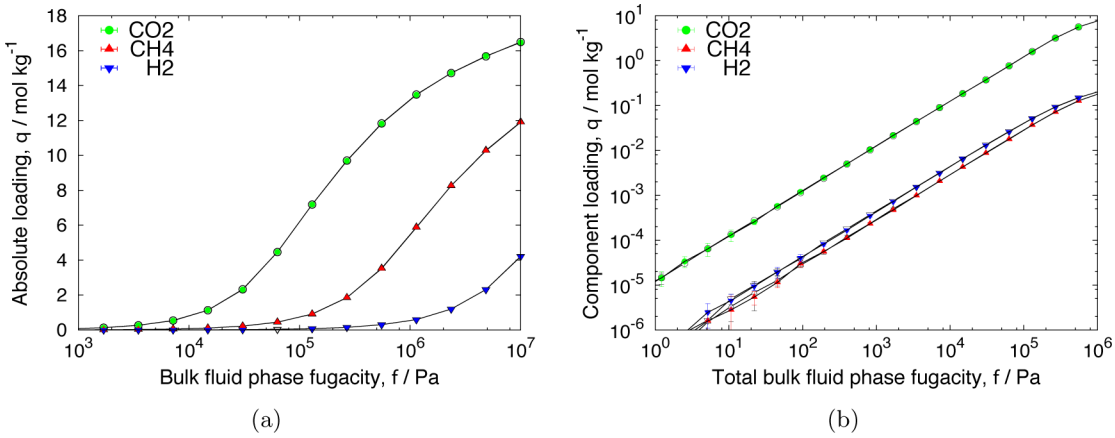

Figure 2. Adsorption isotherms calculated using CFCMC (closed symbols) and CBMC (open symbols). (a) Single-component isotherms of CO_2,CH_4,H_2 in Mg-MOF-74 at 313K. (b) Three-component mixture with a ratio of 1:4:20 CH_4:CO_2:H_2 in Mg-MOF-74 at 313 K.

significant importance in the petrochemical industry. This separation can be achieved by selective adsorption in ordered crystalline nanoporous materials such as zeolites, MOFs, COFs, and ZIFs by exploiting subtle differences in molecular configurations.[46,47] The alkane separation efficiency is generally described by the molecule wall effective distance.[48] Small pore structures like ZIF-77, MFI, and $Fe_2(BDP)_3$[49] can show very large selectivities but have a relatively small pore volume. This class of systems generally favor the adsorption of the linear alkanes. Slightly larger pores show an opposite hierarchy with the dibranched molecules fitting best (e.g., UiO-66), while even larger pores revert back to having the linear alkane adsorb best, albeit with much lower selectivities than the small-pore structures.

In Figure 1, we show CFCMC and CBMC isotherms of hexane isomers at 433 K in $Fe_2(BDP)_3$. $Fe_2(BDP)_3$ is a highly stable framework with one-dimensional triangular channels made of iron and benzene-1,4-dicarboxylic acid (BDP). The crystal data was taken from ref 49, and we used 5 × 1 × 1 unit cells with periodic boundaries. The framework is modeled using the DREIDING force field,[50] and atoms not defined in the DREIDING model are taken from the UFF.[51] The alkanes are modeled using the transferable potentials for phase equilibria (TraPPE) force field by Martin and Siepmann.[20,52] Despite the fact that the model lumps CH_3, CH_2, and CH into single interaction centers, it very accurately reproduces the experimental phase diagram and critical points. Cross interactions are mixed using the Lorentz−Berthelot mixing rule.[53,54]

For both single components as well as the five-component mixture, we find excellent agreement between the CFCMC and the CBMC method. The simulations have been run the same number of cycles (where a cycle consist of N Monte Carlo moves, and N is the number of molecules present in the system with a minimum of 20 moves) and roughly for the same amount of CPU time. We note that for CFCMC, the error bar becomes larger in regions where the isotherms are more steep (however, note the average matches CBMC very well with CBMC). This is an indication that CFCMC is able to explore more phase space than CBMC. Also note that CFCMC matches CBMC even for loadings that are very small. It is the integer number of molecules that is the relevant property, and the fractional molecule should be excluded in the analysis. Our simulations agree both qualitatively and quantitatively with the CBMC simulations of ref 49 further supporting the correctness of the simulation results. From our simulations, we observe that for these flexible molecules with internal degrees of freedom the CFCMC is just as efficient as CBMC.

3.2. Small Gas Molecules in MgMOF-74. The separation of light gases is becoming increasingly important from an energetic and environmental point of view. Separation of CO_2 from CH_4 in natural gas helps reducing CO_2 emission into the atmosphere and increases the energetic value of the gas, while separation of CO_2, CH_4, and H_2 is important in hydrogen flow purifications.[55,56] The separation of these gases can be achieved by adsorption processes using porous materials with high selectivity (such as zeolites, silicas, and MOFs), which exploit the differences in kinetic diameter, polarizability, and dipole and quadrupole moments of the molecules. It has already been reported that materials with open metal sites enhance the binding strength of H_2 and CH_4[56] making them suitable candidates for separation of small gases. Screening studies by, for example, Yazaydin et al.,[57] also showed that MgMOF-74 has a very high CO_2 capacity.

In Figure 2, we show the CFCMC and CBMC adsorption isotherms for CO_2, CH_4, and H_2 at 313 K in MgMOF-74, a metal organic framework with one-dimensional channels and a high concentration of Mg^{2+}. The crystallographic data was taken from ref 56, and a 2 × 2 × 5 unit cell with periodic boundaries was used. The Lennard−Jones parameters for the framework were taken from DREIDING force field. Charges were obtained from quantum calculations (using the REPEAT method.[58]) The interaction parameters for the gas molecules were taken from the TraPPE force field[52,59] in which H_2 is modeled as a rigid molecule with one dispersive center in the center of mass (COM) and partial charges in both hydrogens and the COM, CO_2 as a rigid molecule with three interaction centers with partial charges, and CH_4 as one interaction center. For the mixture isotherms, 1:4:20 CH_4:CO_2:H_2 ratios were used in order to compare with previous results,[60] which model a realistic hydrogen purification process composition. In both cases, we can see excellent agreement between CBMC and CFCMC. There is also good agreement between our results for single components and previously published data.[56]

3.3. Xylenes in MTW. Xylenes is a term that refers to dimethylbenzenes obtained from petroleum and generally produced as a mixture of all three isomers: *ortho*-, *meta*-, and *para*-xylene. The industrial applications of the isomers differ. p-Xylene is the main precursor of polyethylene terephtalate

dx.doi.org/10.1021/ct4009766 | J. Chem. Theory Comput. 2014, 10, 942−952

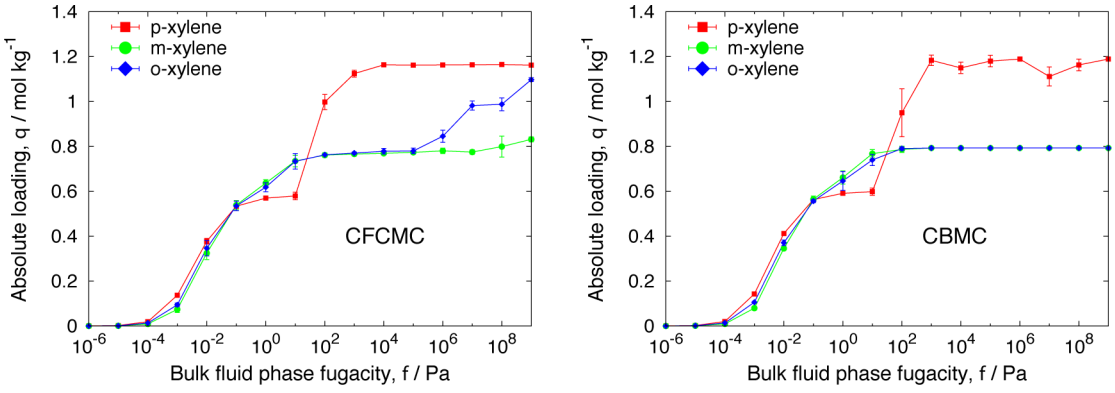

Figure 3. Pure component adsorption isotherms of xylenes isomers in MTW zeolite at 433 K calculated with (a) CFCMC and (b) CBMC.

(PET) for the polyester industry. o-Xylene is used to obtain phtahalic anhydride, and m-xylene is used to produce isophthalic acid in a PET resin blend. Therefore, their separation is of great interest. However, the similarities in the physicochemical properties of xylenes make this process challenging.[61] The current preferred technology is based on adsorption in nanoporous structures,[62] in which energetic and entropic effects are responsible for the selectivity of the different isomers.

In Figure 3, we show the CFCMC and CBMC isotherms of xylenes at 433 K in MTW, a zeolite with one-dimensional channels and 12-rings openings. The crystallographic data was taken from ref 63 and modeled with the DREIDING force field. Interactions with both oxygen and silicon are taken into account. A 1 × 6 × 3 unit cell was used. Xylenes were modeled using the OPLS-UA force field.[64] There is good agreement between CBMC and CFCMC for the single-component isotherms at low pressures; however, at high pressures, CBMC has difficulties with inserting more molecules in the system. This behavior is particularly clear in the case of o-xylene. CBMC simulations will lead to an incorrect maximum loading. We have noticed something similar for small guest molecules at saturation in our previous work.[3]

In Figure 4, we show a snapshot of the mixture adsorption. In the top and bottom channel of MTW, only p-xylenes are present, and we can observe how the molecules are able to efficiently pack by enhancing $\pi-\pi$ interactions. In the middle channel, also an o-xylene and a m-xylene are present. We can observe that these isomers are not able to stack in the same mode. In Figure 5, we can observe how the different isomers interact with the framework. This specific fitting between the xylenes makes the system extremely difficult to sample.

4. LENNARD–JONES CHAINS IN GIBBS ENSEMBLE

To test the continuous fractional Monte Carlo with configurational bias, we computed the coexistence densities for Lennard–Jones chains of length m = 8 and octane using three different algorithms: CBMC, CFCMC, and CB/CFCMC in the Gibbs ensemble. For the algorithms with CBMC, simulations were performed with 10 trial positions. The results for the coexistence densities ($\langle\rho_1\rangle$ and $\langle\rho_2\rangle$) are shown in Tables S2 and S3 of the Supporting Information. For the Lennard–Jones 8-mers, the results are presented in reduced units to compare with the literature. They are in good agreement with each other and with the results reported by ref

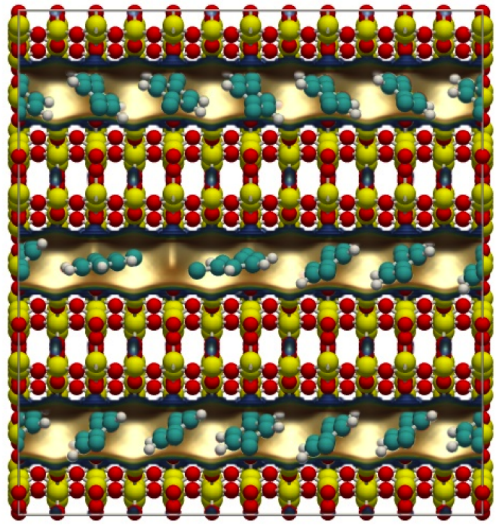

Figure 4. YZ view of MTW channels with an equimolar mixture of xylenes isomers at 10^8 Pa and 433 K. The channels are cut open and volume-rendered based on an energy grid probed with methane. Color code: carbon (cyan), hydrogen (white), oxygen (red), and silicon (yellow).

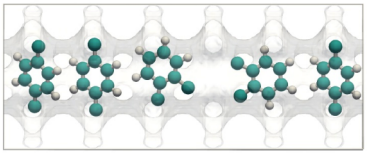

Figure 5. View into one channel of MTW with an equimolar mixture of xylenes isomers at 10^8 Pa and 433 K . The channel shape is a transparent isocontour of a high energy from an energy grid probed with methane. Channel runs from left to right. Color code: carbon (cyan) and hydrogen (white).

12. For the octanes, our results are in good agreement with each other and equivalent within the error bar to the results reported by ref 52.

The gas-phase density value at T^* = 1.923 of Mooij et al.[12] differs from our value. However, this density is lower than the density at T^* = 1.887, which seems inconsistent. Our data points have been run 10 times longer. Considering this difference, the data agree well. However, this raises a discussion on the magnitude of error bars. Our error bars are computed by

dx.doi.org/10.1021/ct4009766 | J. Chem. Theory Comput. 2014, 10, 942–952

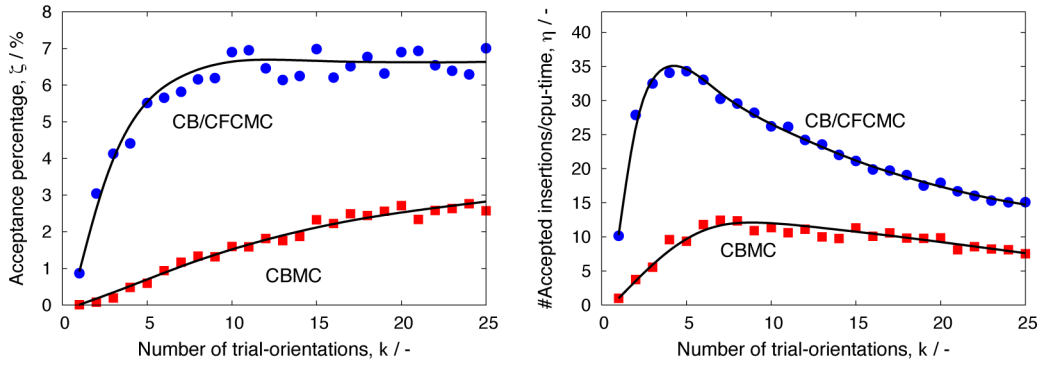

Figure 6. Efficiencies for CBMC, CFCMC, and CB/CFCMC algorithms for Lennard–Jones chains with eight beads. Total number of chain molecules N = 200, temperature T^* = 1.887, and total volume V_t^* = 3456. The number of MC production cycles = 50,000.

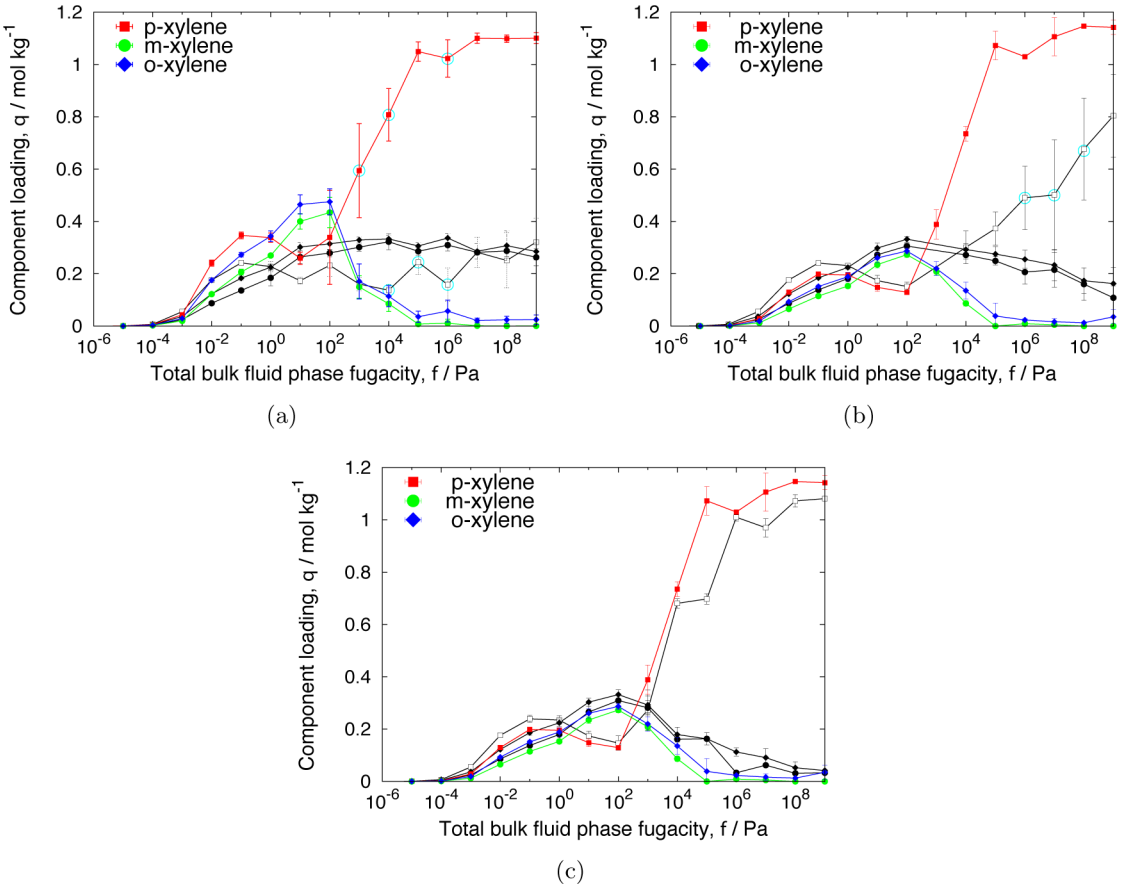

Figure 7. Adsorption isotherms calculated with CFCMC (closed symbols) vs CBMC (open symbols) for a three-component equimolar mixture of xylenes isomers in MTW at 433 K: (a) CFCMC and CBMC 500,000 cycles, (b) CFCMC and CBMC 2,000,000 cycles, and (c) CFCMC 2,000,000 and CBMC 3,000,000 cycles. The circled points are discussed further in the text.

dividing the simulation in five blocks and computing the error from the standard deviation of the averages of these five blocks. We report a 95% confidence interval. In Gibbs simulations, the density fluctuates as the volume, and the number of particles fluctuate individually. The magnitude of the fluctuations are the most sensitive to the frequency and magnitude of the volume move. Longer simulation times give a better estimate of the "true" average but also an increased contribution to the error from exploring a larger region of phase space. In order to evaluate this "hidden" error, it is advisable to plot the full VLW curve and check that the graph is smooth and continuous. This would also reveal that the T^* = 1.923 data point of Mooij et al. can be considered an outlier.

The gas and liquid branches are well separated by a free energy barrier at low temperatures. At high temperature, the barrier becomes low, which makes Gibbs difficult to apply at these temperatures. This manifests itself as swapping between the liquid and gas boxes. This must be avoided to accurately compute the gas and liquid densities separately. However, sometimes the better you sample (i.e., CFCMC and CB/CFCMC), the more probable the swapping becomes.

The performance and efficiency of the CB/CFCMC algorithm in the Gibbs ensemble can be assessed by computing

dx.doi.org/10.1021/ct4009766 | J. Chem. Theory Comput. 2014, 10, 942−952

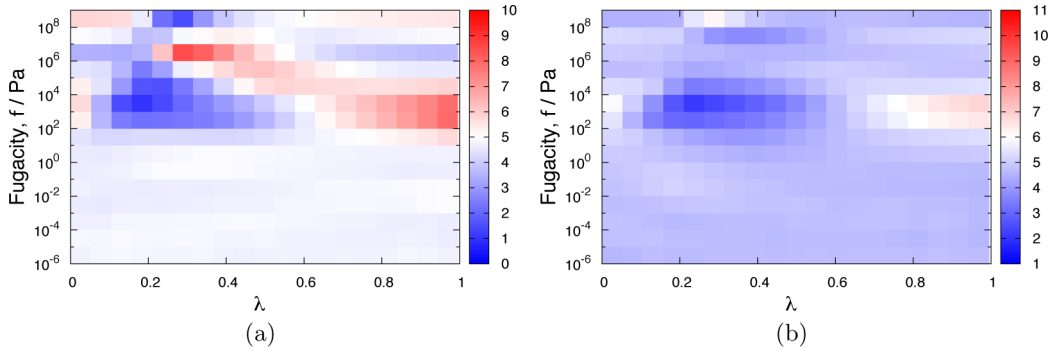

Figure 8. Probability distributions of λ at different fugacities for p-xylene in MTW at 433 K measured in production time after using Wang−Landau (a) 2,000,000 cycles and (b) 3,000,000 cycles.

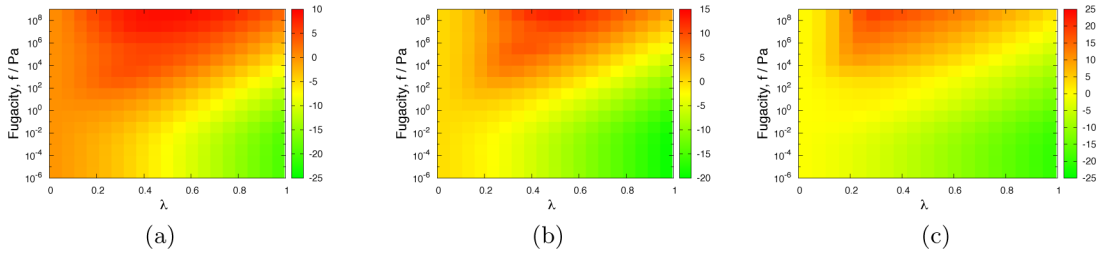

Figure 9. Biasing factors in units of k_BT at different fugacities for single-component (a) o-xylene, (b) m-xylene, and (c) p-xylene in MTW at 433 K.

the number of accepted particle exchanges between the boxes per Monte Carlo cycles performed and also the number of accepted particle exchanges between the boxes per total CPU time for the different algorithms. Moves are chosen with the following probabilities: Gibbs volume 0.2%, translation 19.96%, rotation 19.96%, reinsertion 19.96%, partial reinsertion 19.96%, and Gibbs swap 19.96%. For the CFCMC and CB/CFCMC, the number of accepted particle exchanges are defined as the total number of accepted moves in λ that result in particle exchanges between the boxes. The measured time is the time of just the Gibbs insertion/deletion move for an insertion. The clock routine was used that measured only CPU time. We ran on a 12-core machine using 10 jobs simultaneously (and with two cores free for system tasks) to make sure none of them can make use of the cache (or at least all used the same cache). The results for the number of accepted particle exchanges per MC cycle and per CPU Time for the different algorithms for Lennard−Jones chains with 8 beads are presented in Figure 6.

We can observe that, as expected, the amount of accepted exchanges per MC cycle for both CBMC and CB/CFCMC increases with the number of trial positions. CB/CFCMC increases significantly the amount of acceptance percentage with respect to CBMC. In CBMC, the efficiency as a function of the number of trial directions has not a pronounced maximum but rather a broad plateau, while for CB/CFCMC, there is a pronounced maximum at only a few trial directions. The acceptance probability cannot exceed 50% because of the choice of $\Delta\lambda$, so that having more trial directions (than the optimum) results in a decrease in acceptance. Note that we fixed λ_{max} = 0.332 and fixed the biasing factors for all runs.

5. EFFICIENCY OF CFCMC

To assess the efficiency of CFCMC, we considered the system of xylenes in MTW because sampling this system for mixtures turned out to be very difficult. An interesting property of the single-component isotherms is that p-xylene has an inflection point in its loading at approximately 10 Pa (Figure 3), which causes it to have a lower loading than m- and o-xylene within a small fugacity range. This sampling difficulty is reflected in Figure 7, where the mixture comparison between CFCMC and CBMC is plotted.

In Figure 7(a), for the simulation time of 500,000 initialization and 500,000 production cycles, we observe that CFCMC and CBMC give very different answers. The questions are as follows: "Which one is more correct than the other, and/or are both methods giving wrong answers here?" We have run the simulation using both methods longer, and in Figure 7(b), we observe that CFCMC provides the same qualitative answer and a slightly improved quantitative result, while Figure 7(b) and (c) show that when running CBMC (much) longer, CBMC converges to the CFCMC result. This means that CFCMC is able to provide qualitative correct results in short simulation times, while CBMC is easily stuck/trapped in metastable states. Hence, CFCMC is not only more efficient, it is for all but the shortest simulation almost guaranteed to find the proper solution (if biasing is used with appropriate biasing factors).

Because biasing is so essential, we analyze this in some more detail. In Figure 8, we plot the λ histograms for 2,000,000 and 3,000,000 equilibration cycles. During equilibration of λ, the histograms are measured and used to calibrate the biasing factors using Wang−Landau method. Ideally, the final histograms should be flat. In Figure 8(a), we observe that the histograms are reasonably flat, but in Figure 8(b), the histograms become increasingly flat with longer calibration times (more details are given in Figures S2 and S3, Supporting Information). The latter histograms are sufficiently flat to appropriately analyze the biasing factors. If the histograms would be completely flat, then the difference of the biasing factor at λ = 0 and λ = 1 is the free energy difference of inserting a molecule,[6] and therefore, it increases with increasing molecule size. Moreover, a flat histogram indicates that most

dx.doi.org/10.1021/ct4009766 | J. Chem. Theory Comput. 2014, 10, 942−952

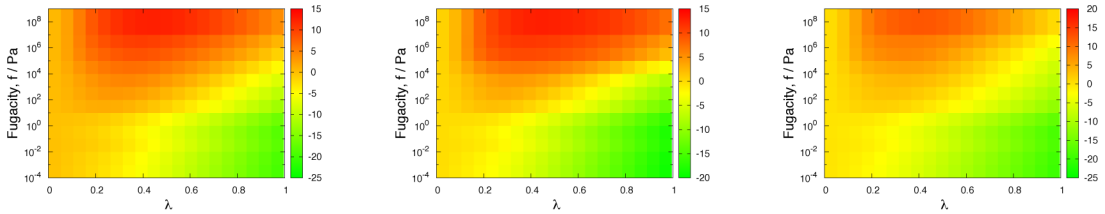

Figure 10. Biasing factors in units of k_BT at different fugacities for (a) o-xylene, (b) m-xylene, and (c) p-xylene in MTW at 433 K in a equimolar ternary mixture.

free energy barriers in λ space have been eliminated. This leads to an order of magnitude better insertion efficiency. Not only is the insertion "forced" but also the adjustment of the surrounding molecules. It is this adjustment that is so difficult to sample with CBMC, especially with "packing-effects" like those shown in Figure 5. For the three-component xylene mixture, the individual loadings are determined by the relative differences between the components. Seen from the viewpoint of a particular molecule, there is a preferred packing of molecules around it. This preference changes as a function of loading. Because one always starts from either the zero loading or a previously stored nonequilibrated snapshot (for example at a lower pressure), the system needs to adjust to the new pressure, and there is a change in free energy between this and the state that one would like to compute. Using CFCMC, the free energy barrier is largely removed, while it is very difficult for CBMC to overcome this barrier. As we will see, these barriers are very large.

In Figures 9 and 10, the biasing factors for the single-component o-, m-, and p-xylene and the mixture are plotted as a function of λ and fugacity. It is important to note that for each fugacity the biasing factor is taken as zero for $\lambda = 0$, and the nonzero λ biasing factors are relative to this value. At low fugacities, increasing λ leads to lower biasing values. This corresponds to the regime where increasing the molecule gains energy, that is, the interaction of the framework (and other molecules in general) with the fractional molecule is very favorable and increasing λ leads to lower free energies. If we increase the fugacity, we start to feel the effect of loading. At a certain point, the surrounding molecules start to become a repulsive influence. Increasing the loading even further, we observe that there appears a λ bottleneck somewhere at an intermediate λ value, that is, a minimum in λ space . This free energy barrier is also related to the barrier for an orientational rearrangement of the molecules. One pushes the fractional molecule in but halfway and the other molecules need to adapt to the new situation. In CBMC simulations, the molecule would have been removed immediately (because it is energetically very unfavorable), but by forcing it to remain, one forces the environment to respond. This process is not very different for the mixtures as shown in Figure 10. The biasing plots for alkanes in $Fe_2(BDP)_3$ and small gases in MgMOF-74 can be found in the Figures S4 and S5 of the Supporting Information. We note that the magnitude of the biasing is much lower, which indicates these systems are feasible to sample with both CFCMC *and* CBMC. The magnitude of the required biasing factors is directly proportional to the difficulty of sampling the system.

In Table 1, we show the average number of molecules in the zeolite for some simulations (circled points, Figure 7) in different stages. The simulation is divided into five blocks, and

Table 1. Average Loading of Molecules per Simulation in Blocks of Cycles

simulation	fugacity 1	fugacity 2	fugacity 3
CBMC (Figure 7(a))	**10^4 (Pa)**	**10^5 (Pa)**	**10^6 (Pa)**
block 1	10.3	9.3	10.1
block 2	10.0	9.1	10.4
block 3	9.7	9.6	10.5
block 4	10.0	9.0	9.9
block 5	10.2	9.1	9.8
CFCMC (Figure 7(a))	**10^3 (Pa)**	**10^4 (Pa)**	**10^6 (Pa)**
block 1	21.2	24.5	29.4
block 2	21.1	23.7	32.4
block 3	14.5	22.2	31.6
block 4	16.8	24.9	30.0
block 5	16.1	26.8	31.2
CBMC (Figure 7(b))	**10^6 (Pa)**	**10^7 (Pa)**	**10^8 (Pa)**
block 1	12.5	11.0	16.4
block 2	13.7	12.6	18.1
block 3	14.4	15.6	20.3
block 4	15.6	16.1	23.8
block 5	17.8	20.3	23.6

if all five averages show a systematic increase in loading, then the loading values are not yet converged. In Table 1, we show that for short simulations of CBMC the average number of molecules has small fluctuations. This however does not mean the simulations are equilibrated; as mentioned before, this is only a consequence of the system being trapped in a metastable state. For longer simulations of CBMC, the average number of molecules has large changes (which is reflected by the error bars in Figure 7(b)). However, we can notice the loading is drifting upward, so the simulations are clearly not converged. For CFCMC, the average loading has large fluctuations with no obvious direction. This together with a flat enough λ histogram indicates that the system is exploring large regions in phase space around the correct average loadings.

6. CONCLUSIONS

The efficiency of insertion depends on the density of the system. At low densities and for a fixed number of Monte Carlo cycles, CBMC is more efficient because the attempts of insertion are more frequent; no diffusion in λ space is needed. At medium densities, the efficiency of insertion can be summarized by CB/CFCMC $\gg$ CFCMC $\gg$ CBMC $\gg$ MC. Methods using CFCMC really shine because they are rather insensitive to metastable states because of the λ biasing. A molecular structure or packing can be broken down if the λ histogram is relatively flat. This requires an equilibration period during which the λ biasing is iteratively setup using, for example, Wang–Landau sampling, but in our experience, this

dx.doi.org/10.1021/ct4009766 | J. Chem. Theory Comput. 2014, 10, 942–952

does not require *longer* equilibration. After a simulation, the λ histogram can be examined. If it is relatively flat, then block averages are an indication of equilibration. In contrast, CBMC can show a small error bar, no drift in block averages, and can still be unconverged.

In addition, CB/CFCMC has a clear advantage for long-chain molecules because it avoids having to generate ideal gas configurations for the CFCMC insertions. Although this generation might be cheap, for increasing chain lengths, the molecular configurations inside the host framework increasingly deviate from their ideal gas configuration. The CFCMC would fail here, while the CB/CFCMC could still work by growing the molecule atom by atom.

However, the CB/CFCMC and CFCMC are not applicable around saturation conditions. For relatively large pores systems, the fluid inside the pores can be compressed further and further with no bounds (in practice, the bound is the maximum pressure the experimental equipment can handle and/or the nanoporous material remains stable), but for small pores and relatively bulky molecules (using hard potentials), the saturation can be an *integer* number of molecules. A typical example is a xylene in UiO-66 or a heptane molecule in an ERI-type zeolite. There fits only one heptane molecule in an ERI-type cage at reasonable pressures. For these cases, it is impossible to insert an additional molecule at saturation conditions, and similarly, at saturation, it is energetically highly unfavorable to delete a molecule. In this case, however, for single components, the loading is known, and for mixtures, it is the ratio of components that is of interest. This ratio is better sampled using MC moves like identity switches or methods like replica exchange in temperature or mol-fraction.[65] Alternatively, especially when simulating flexible hosts, sampling efficiency can be gained by combing the insertion/deletion schemes with the MD methodology.

■ ASSOCIATED CONTENT

Supporting Information

We derived the acceptance rules for CB/CFCMC and present the validation data. This includes single component and mixtures isotherms for alkanes in $Fe_2(BDP)_3$ and tables with the vapor−liquid coexistence densities for Lennard−Jones chains and octane computed in Gibbs ensemble. Details on the λ histograms for xylenes in MTW and plots for the biasing factors of small gases in MgMOF-74 and alkanes in $Fe_2(BDP)_3$ and a general description on the use of grids for calculating the energies are also included. This material is available free of charge via the Internet at http://pubs.acs.org.

■ AUTHOR INFORMATION

Corresponding Author

*E-mail: D.Dubbeldam@uva.nl.

Notes

The authors declare no competing financial interest.

■ ACKNOWLEDGMENTS

This material is supported by The Netherlands Research Council for Chemical Sciences (NWO/CW), also through a VIDI grant (David Dubbeldam), and by the Stichting Nationale Computerfaciliteiten (National Computing Facilities Foundation, NCF) for the use of supercomputing facilities. It is also performed as part of the CATO-2 program, the Dutch national RandD program on CO_2 capture, transport, and storage, funded by the Dutch Ministry of Economic Affairs (Sayee Prasaad Balaji). We thank C. N. van Dijk for comments on the manuscript.

■ REFERENCES

(1) Allen, M. P.; Tildesley, D. J. *Computer Simulation of Liquids*; Clarendon Press: Oxford, 1987.
(2) Frenkel, D.; Smit, B. *Understanding Molecular Simulation*, 2nd ed.; Academic Press: London, 2002.
(3) Dubbeldam, D.; Torres-Knoop, A.; Walton, K. S. *Mol. Simul.* **2013**, *39:14−15*, 1253−1292.
(4) Siepmann, J. I.; Frenkel, D. *Mol. Phys.* **1992**, *75*, 59−70.
(5) Rosenbluth, M. N.; Rosenbluth, A. W. *J. Chem. Phys.* **1955**, *23*, 356−359.
(6) Shi, W.; Maginn, E. J. *J. Chem. Theory Comput.* **2007**, *3*, 1451−1463.
(7) Shi, W.; Maginn, E. J. *J. Comput. Chem.* **2008**, *29*, 2520−2530.
(8) Rosch, T. W.; Maginn, E. J. *J. Chem. Theory Comput.* **2011**, *7*, 269−279.
(9) Dubbeldam, D.; Calero, S.; Ellis, D. E.; Snurr, R. Q. *RASPA 1.0: Molecular Software Package for Adsorption and Diffusion in Flexible Nanoporous Materials*, 1.0-alpha ed.; Northwestern University: Evanston, IL, 2013.
(10) Harris, J.; Rice, S. A. *J. Chem. Phys.* **1988**, *88*, 1298−1307.
(11) Siepmann, J. I. *Mol. Phys.* **1990**, *70*, 1145−1158.
(12) Frenkel, D.; Mooij, G. C. A. M.; Smit, B. *J. Phys.: Condens. Matter* **1992**, *4*, 3053−3076.
(13) de Pablo, J. J.; Suter, M.; Suter, U. W. *J. Chem. Phys.* **1992**, *96*, 2395−2403.
(14) Laso, M.; de Pablo, J. J.; Suter, U. W. *J. Phys.: Condens. Matter* **1992**, *97*, 2817−2819.
(15) de Pablo, J. J.; Siepmann, J. I.; McDonald, I. R. *Mol. Phys.* **1992**, *75*, 255−259.
(16) Panagiotopoulos, A. Z. *Int. J. Thermophys.* **1989**, *10*, 447−457.
(17) de Pablo, J. J.; Prausnitz, J. M. *Fluid Phase Equilib.* **1989**, *53*, 177−189.
(18) Panagiotopoulos, A. Z. In *Observation, Prediction and Simulation of Phase Transitions in Complex Fluids*; Baus, M., Rull, L.R., Ryckaert, J. P., Eds.; Vol. NATO ASI Series C; Kluwer Academic: The Netherlands, 1995; Vol. *460*, pp 463−501.
(19) Martin, M. G.; Siepmann, J. I. *J. Am. Chem. Soc.* **1997**, *119*, 8921−8924.
(20) Martin, M. G.; Siepmann, J. I. *J. Phys. Chem. B* **1999**, *103*, 4508−4517.
(21) Chen, B.; Siepmann, J. I. *J. Phys. Chem. B* **1999**, *103*, 5370−5379.
(22) Macedonia, M. D.; Maginn, E. J. *Mol. Phys.* **1999**, *96*, 1375−1390.
(23) Vlugt, T. J. H.; Krishna, R.; Smit, B. *J. Phys. Chem. B* **1999**, *103*, 1102−1118.
(24) Vlugt, T. J. H.; Martin, M. G.; Smit, B.; Siepmann, J. I.; Krishna, R. *Mol. Phys.* **1998**, *94*, 727−733.
(25) Vlugt, T. J. H. *Mol. Simulat.* **1999**, *23*, 63−78.
(26) Consta, S.; Vlugt, T. J. H.; Hoeth, J. Wichers; Smit, B.; Frenkel, D. *Mol. Phys.* **1999**, *97*, 1243−1254.
(27) Deem, M. W.; Bader, J. S. *Mol. Phys.* **1996**, *87*, 12451260.
(28) Wick, C. D.; Siepmann, J. I. *Macromolecules* **2000**, *33*, 7207−7218.
(29) Uhlherr, A. *Macromolecules* **2000**, *33*, 13511360.
(30) Shah, J. K.; Maginn, E. J. *J. Chem. Phys.* **2011**, *135*, Artn. 134121.
(31) Jakobtorweihen, S.; Lowe, C. P.; Keil, F. J.; Smit, B. *J. Chem. Phys.* **2006**, *124*, 154706.
(32) Martin, M. G.; Frischknecht, A. L. *Mol. Phys.* **2006**, *104*, 2439−2456.
(33) Martsinovski, A. P.; Lyubartsev, A. A.; Shevkunov, S. V.; Vorontsov-Velyaminov, P. N. *J. Chem. Phys.* **1992**, *96*, 1776−1783.
(34) Escobedo, F. A.; de Pablo, J. J. *J. Chem. Phys.* **1996**, *105*, 4391−4394.

(35) Duane, S.; Kennedy, A. D.; Pendleton, B. J.; Roweth, D. *Phys. Lett. B* **1987**, *195*, 216−222.
(36) Chempath, S.; Clark, L. A.; Snurr, R. Q. *J. Chem. Phys.* **2003**, *118*, 7635−7643.
(37) Wang, F.; Landau, D. P. *Phys. Rev. E* **2001**, *64*, 056101.
(38) Wang, F.; Landau, D. P. *Phys. Rev. Lett.* **2001**, *86*, 2050−2053.
(39) Vlugt, T. J. H.; Schenk, M. *J. Phys. Chem. B* **2002**, *106*, 12757−12763.
(40) June, R. L.; Bell, A. T.; Theodorou, D. N. *J. Phys. Chem.* **1990**, *94*, 8232−8240.
(41) Snurr, R. Q.; June, R. L.; Bell, A. T.; Theodorou, D. N. *Mol. Simulat.* **1991**, *8*, 73−92.
(42) Schultz, M. *Spline Analysis*; Prentice Hall: Englewood Cliffs, NJ, 1973.
(43) Lekien, F.; Marsden, J. *Int. J. Numer. Methods Eng.* **2005**, *63*, 455−471.
(44) Press, W. H.; Flannery, B. P.; Teukolsky, S. A.; Vetterling, W. T. *Numerical Recipes in C*; Cambridge University Press: New York, 1988.
(45) Vlugt, T. J. H.; Garcia-Perez, E.; Dubbeldam, D.; Ban, S.; Calero, S. *J. Chem. Theory. Comput.* **2008**, *4*, 1107−1118.
(46) Maesen, T. L. M.; Beerdsen, E.; Calero, S.; Dubbeldam, D.; Smit, B. *J. Catal.* **2006**, *237*, 278−290.
(47) Smit, B.; Maesen, T. L. M. *Nature* **1995**, *374*, 42−44.
(48) Dubbeldam, D.; Krishna, R.; Calero, S.; Yazaydin, A. O. *Angew. Chem., Int. Ed.* **2012**, *51*, 1186711871.
(49) Herm, Z. R.; Wiers, B. M.; Mason, J. A.; van Baten, J. M.; Hudson, M. R.; Zajdel, P.; Brown, C. M.; Masciocchi, N.; Krishna, R.; Long, J. R. *Science* **2013**, *340*, 960−964.
(50) Mayo, S. L.; Olafson, B. D.; Goddard, W. A. *J. Phys. Chem.* **1990**, *94*, 8897−8909.
(51) Rappé, A. K.; Casewit, C. J.; Colwell, K. S.; Goddard, W. A.; Skiff, W. M. J. *J. Am. Chem. Soc.* **1992**, *114*, 10024−10035.
(52) Martin, M. G.; Siepmann, J. I. *J. Phys. Chem. B* **1998**, *102*, 2569−2577.
(53) Lorentz, H. A. *Ann. Phys.* **1881**, *12*, 127−136.
(54) Berthelot, D. *C. R. Hebd. Sceances Acad. Sci.* **1898**, *126*, 1703−1855.
(55) Peng, X.; Cheng, X.; Cao, D. *J. Mater. Chem.* **2011**, *21*, 11259−11270.
(56) Wu, H.; Zhou, W.; Yildirim, T. *J. Am. Chem. Soc.* **2009**, *131*, 4995−5000.
(57) Yazaydin, A. O.; Snurr, R. Q.; Park, T. H.; Koh, K.; Liu, J.; LeVan, M. D.; Benin, A. I.; Jakubczak, P.; Lanuza, M.; Galloway, D. B.; Low, J. J.; Willis, R. R. *J. Am. Chem. Soc.* **2009**, *131*, 18198−18199.
(58) Campana, C.; Mussard, B.; Woo, T. K. *J. Chem. Theory Comput.* **2009**, *5*, 2866−2878.
(59) Potoff, J. J.; Siepmann, J. I. *AIChE J.* **2001**, *47*, 1676−1682.
(60) Herm, Z. R.; Krishna, R.; Long, J. R. *Microporous Mesoporous Mater.* **2012**, *151*, 481−487.
(61) Castillo, J. M.; Vlugt, T. J. H.; Calero, S. *J. Phys. Chem. C* **2009**, *113*, 20869−20874.
(62) Santos, K. A. O.; Dantas Neto, M. C. P. A. A. A.; Moura; Castro Dantas, T. N. *Braz. J. Pet. Gas* **2011**, *5*, 255−268.
(63) Fyfe, C. A.; Gies, H.; Kokotailo, G. T.; Marler, B.; Cox, D. E. *J. Phys. Chem.* **1990**, *94*, 3718−3721.
(64) Jorgensen, W. L.; Tirado-Rives, J. *J. Am. Chem. Soc.* **1988**, *110*, 16571660.
(65) Qiao, Z.; Torres-Knoop, A.; Fairen-Jimenez, D.; Dubbeldam, D.; Zhoua, J.; Snurr, R. Q. *AIChE* **2013**, accepted.